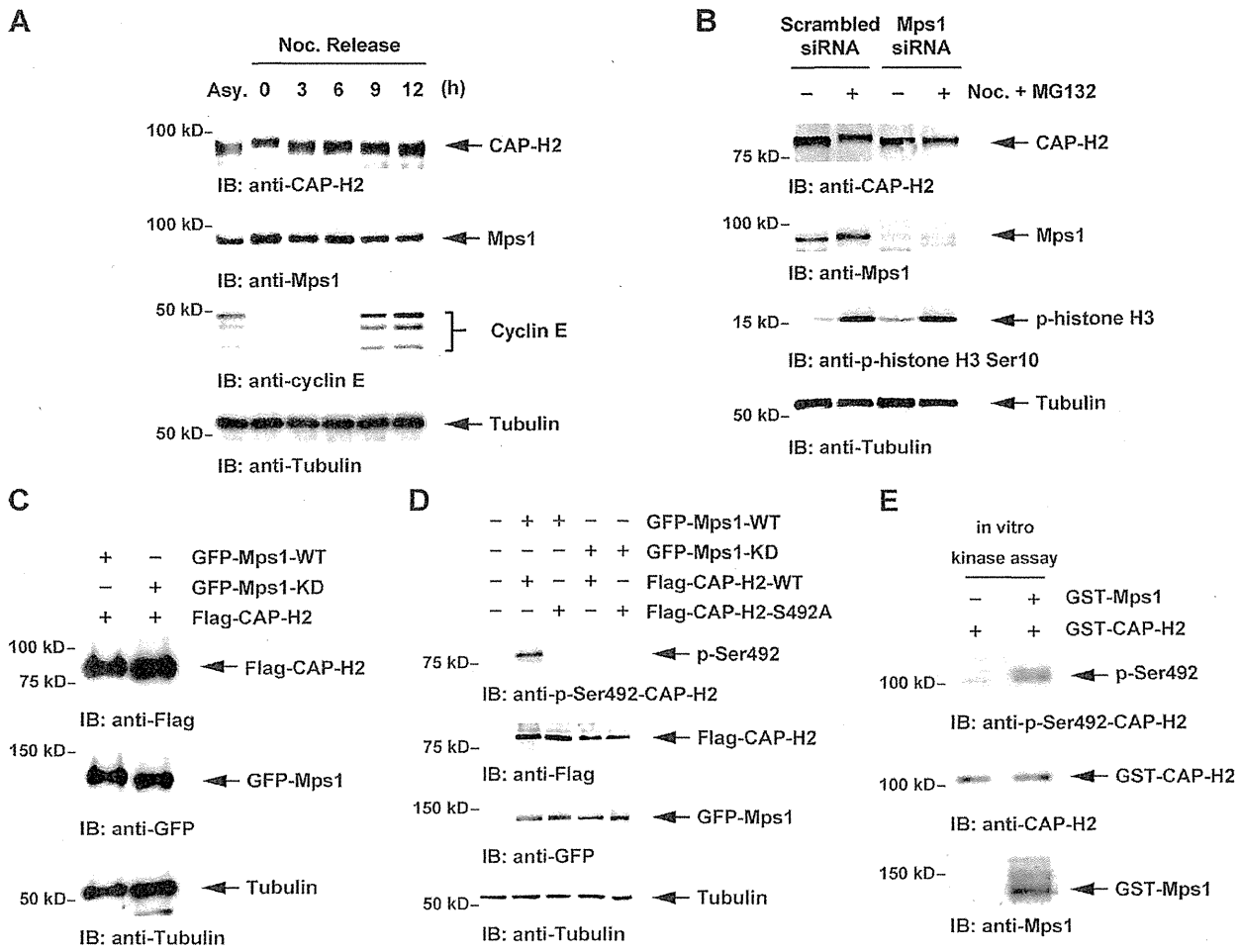

Figure 2. **Identification of Ser492 of CAP-H2 as an Mps1 phosphorylation site.** (A) HeLa cells were treated with nocodazole and released for the indicated times. Lysates were immunoblotted with the indicated antibodies. (B) HeLa cells were transfected with scrambled siRNA or Mps1 siRNA. At 20 h after transfection, cells were treated with DMSO or nocodazole for 16 h and then treated with MG132 for 1 h. Lysates were immunoblotted with the indicated antibodies. (C) 293 cells were cotransfected with GFP-Mps1-WT or GFP-Mps1-KD and Flag-CAP-H2. Cell lysates were immunoblotted with the indicated antibodies. (D) 293 cells were cotransfected with GFP-Mps1-WT or GFP-Mps1-KD and Flag-CAP-H2-WT or Flag-CAP-H2-S492A. Cell lysates were immunoblotted with the indicated antibodies. (E) Recombinant GST-CAP-H2 was incubated with ATP in the presence or absence of GST-Mps1. The reaction products were analyzed by immunoblotting with the indicated antibodies.

Ser492 phosphorylation is required for the targeting of condensin II to mitotic chromosomes

To further examine the significance of the Mps1-dependent phosphorylation of CAP-H2, we generated cell lines that stably express GFP, GFP-tagged CAP-H2 (GFP-CAP-H2-WT), or the S492A mutant (GFP-CAP-H2-S492A). Of note, GFP-CAP-H2 was a resistant form against CAP-H2 siRNA (Fig. 4 A). Both the wild type and mutant CAP-H2 could form condensin complexes in cells (Fig. 4 B), and Ser492 was phosphorylated in wild type, but not S492A mutant during mitosis (Fig. 4 C). To investigate whether Ser492 phosphorylation controls the targeting of condensin II onto mitotic chromosomes, GFP-CAP-H2 stable cell lines were transfected with CAP-H2 siRNA followed by nocodazole treatment. Chromosome fractionation and immunoblot analyses revealed that GFP-CAP-H2-WT largely localized to mitotic chromosomes (Fig. 4 D). In contrast, the S492A mutant was observed in the soluble fraction (unbound chromosome fraction) and impaired its recruitment to chromosomes (Fig. 4 D). Moreover, a fluorescence microscopic analysis using fixed cells demonstrated that although GFP-CAP-H2-WT primarily accumulates in mitotic chromosomes, the S492A mutant showed a defect in chromosome localization (Fig. 4, E and F). Similar results were obtained with living cells (Fig. S3 B). These findings suggest that the association of condensin II with mitotic chromosomes is dependent on Ser492 phosphorylation of CAP-H2 by Mps1.

Mps1 regulates chromosome condensation in the early phase of mitosis

Previous studies have shown that chromosome condensation during prophase is reduced by the depletion of condensin II (Hirota et al., 2004; Ono et al., 2004). In this regard, we investigated whether Mps1 regulates chromosome condensation at

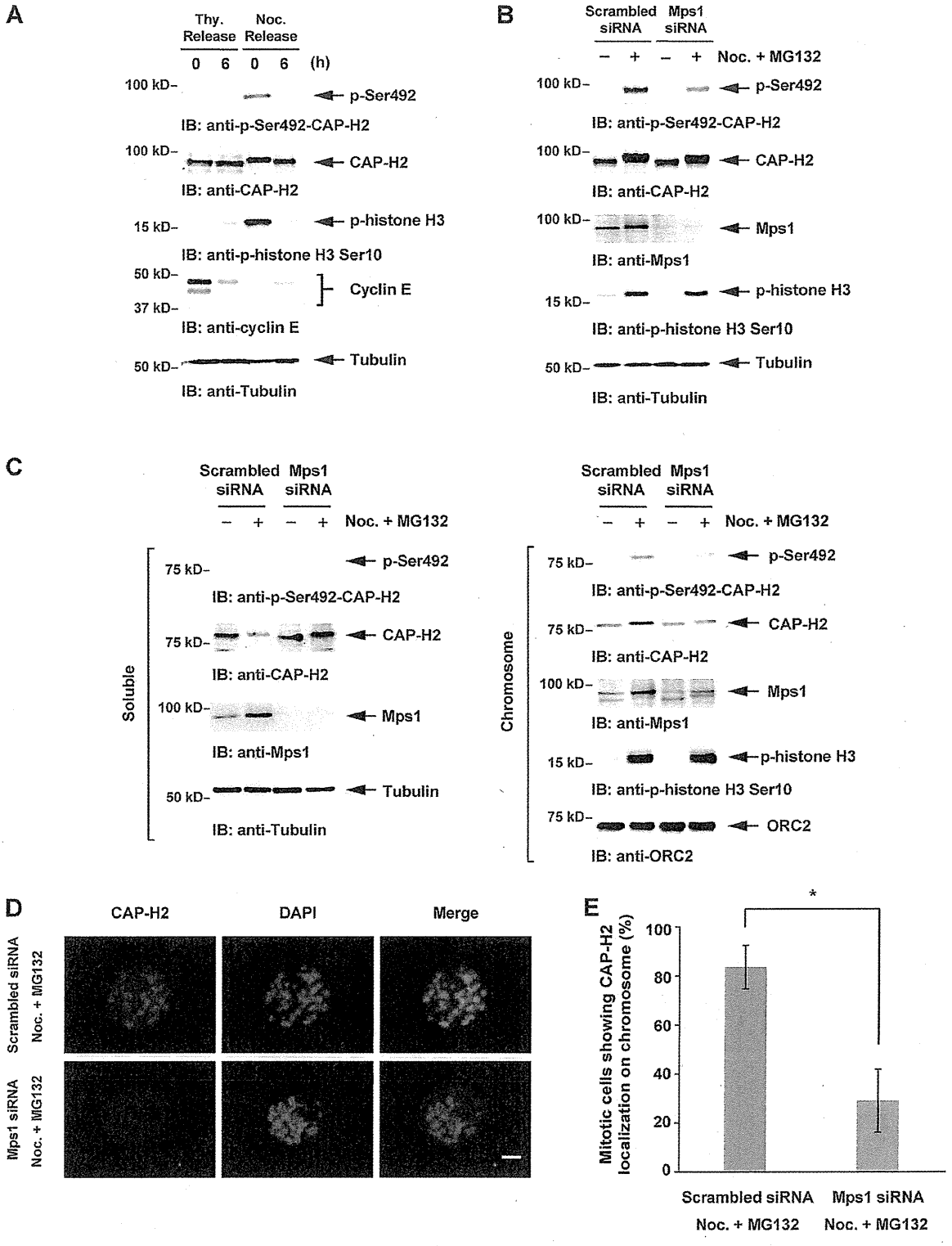

Figure 3. **Mps1 regulates the chromosomal localization of condensin II during mitosis.** (A) HeLa cells were synchronized by double thymidine block or nocodazole and released for the indicated times. Lysates were immunoblotted with the indicated antibodies. (B and C) HeLa cells were transfected with scrambled siRNA or Mps1 siRNA. These cells were synchronized by nocodazole and then treated with MG132. Cell lysates (B) or soluble or chromosome fractions (C) were immunoblotted with the indicated antibodies. (D) HeLa cells were transfected with scrambled siRNA or Mps1 siRNA. These cells were synchronized by nocodazole and then treated with MG132. The mitotic cells were fixed and the spread chromosomes were stained with anti–CAP-H2 (green). DNA was stained by DAPI (blue). Bar, 20 μm. (E) The percentage of cells with CAP-H2 localization on mitotic chromosomes was calculated. Data represent the mean ± SD from three independent experiments (*, $P < 0.05$).

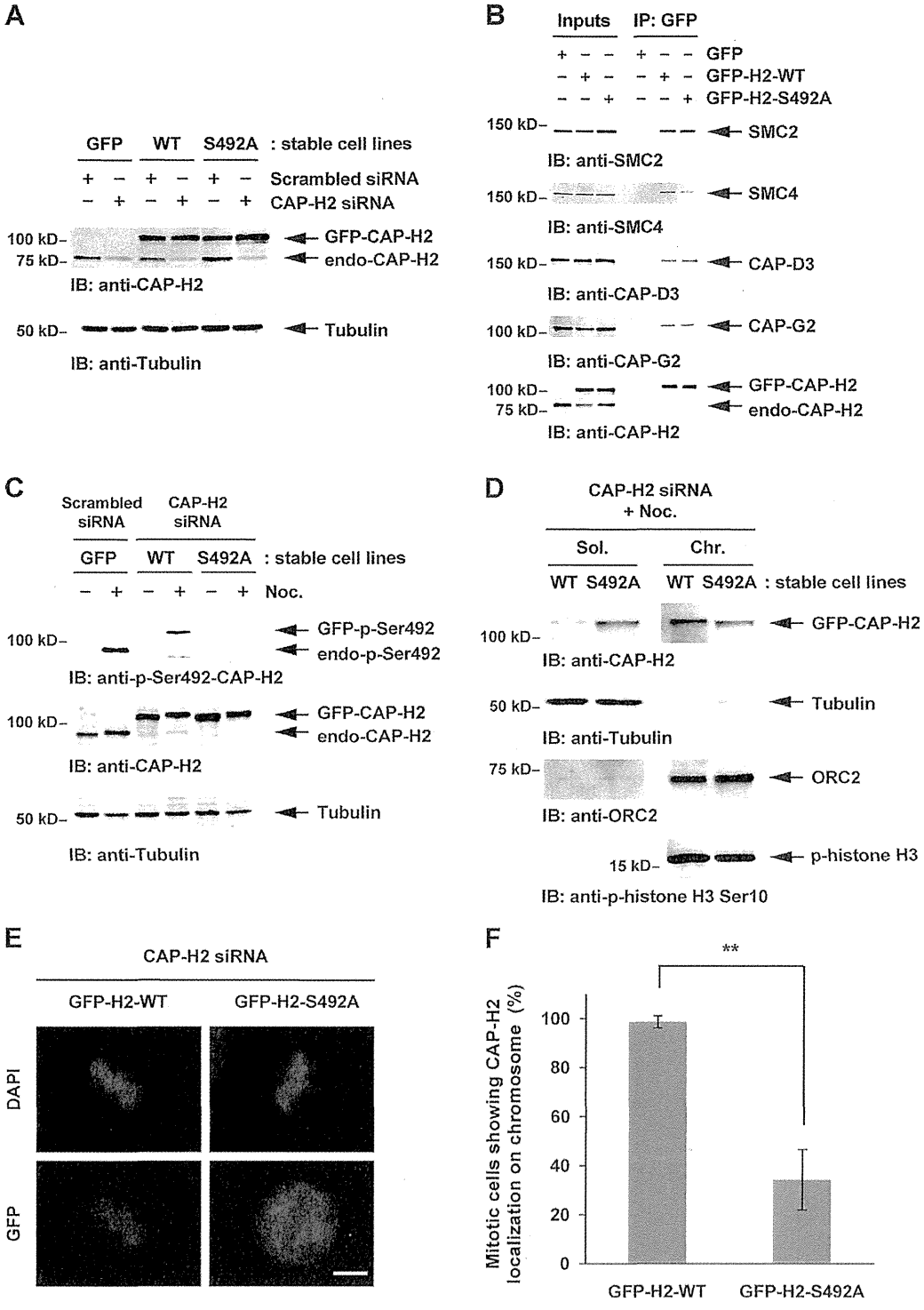

Figure 4. **Ser492 phosphorylation is required for the chromosomal localization of condensin II.** (A) HeLa cells stably expressing GFP (GFP), GFP-CAP-H2-WT (WT), or GFP-CAP-H2-S492A (S492A) were transfected with scrambled siRNA or CAP-H2 siRNA. Lysates were immunoblotted with the indicated antibodies. (B) Lysates from GFP, WT, or S492A cell lines were immunoprecipitated with anti-GFP and were immunoblotted with the indicated antibodies. (C) GFP, WT, or S492A cell lines were transfected with scrambled siRNA or CAP-H2 siRNA followed by treatment with DMSO or nocodazole. Cell lysates were analyzed by immunoblotting with the indicated antibodies. (D) WT or S492A cell lines were transfected with CAP-H2 siRNA followed by nocodazole treatment. The soluble protein fractions (Sol.) and the chromosome fractions (Chr.) were subjected to immunoblotting with the indicated antibodies. (E) WT or S492A cell lines were transfected with CAP-H2 siRNA and fixed. DNA was stained by DAPI. Bar, 10 μm. (F) The percentage of cells with GFP-CAP-H2 localization on mitotic chromosomes was calculated. Data represent the mean ± SD from three independent experiments (**, $P < 0.01$).

prophase. HeLa cells were transfected with scrambled siRNA, Mps1 siRNA, or CAP-H2 siRNA. As reported previously (Ono et al., 2004), prophase cells were monitored by the phosphorylation of histone H3 at Ser10 and by an intact nuclear envelope. The degree of prophase condensation was defined as two categories. In the "weak" category, DAPI and the phospho-histone H3 signal were uniformly distributed in the nucleus (Fig. 5 A, weak). In the "strong" category, a thread-like structure was clearly visible by both DAPI and phospho-histone H3 staining (Fig. 5 A, strong). In contrast to scrambled siRNA-transfected cells, the degree of chromosome condensation during prophase was less in each of the Mps1-depleted cells and CAP-H2–depleted cells (Fig. 5, B and C). To further confirm these results, siRNA-transfected cells were synchronized at G1/S phase and then released. These cells were fixed and prophase condensation was analyzed. The results demonstrated that prophase condensation is reduced by Mps1 and CAP-H2 siRNA (Fig. S3, C and D). Notably, the population of prophase in mitotic cells remained unchanged, indicating that duration of prophase is not affected by Mps1 siRNA or CAP-H2 siRNA (Fig. S3 E). These results thus suggest that the initial phase of mitotic chromosome condensation is induced, at least in part, by Mps1. To investigate the significance of Mps1-mediated phosphorylation of CAP-H2 at Ser492 during early chromosome condensation, we analyzed chromosome condensation during prophase in fixed GFP-CAP-H2 cell lines. As shown previously, a reduction in prophase chromosome condensation was observed in CAP-H2–depleted control cells (Fig. 5, D and E). Importantly, this reduction was rescued by the expression of GFP-CAP-H2-WT and there was little if any effect on the expression of S492A mutant (Fig. 5 D). These results indicate that prophase chromosome condensation by condensin II requires Ser492 phosphorylation. Taken together, these findings support the model in which Mps1 phosphorylates Ser492 of CAP-H2 to control the chromosomal targeting of condensin II for proper chromosome condensation during the initial phase of mitosis (Fig. 5 F).

Mps1 controls chromosome condensation to maintain genome stability

Our results clearly show that Mps1 can phosphorylate CAP-H2 at Ser492 and regulates the localization of condensin II to the mitotic chromosome (Figs. 3 D and 4 E). This is one of the phosphorylations on CAP-H2 because the depletion of Mps1 did not completely abolish the mitotic mobility shift of CAP-H2 (Figs. 3 B and 4 C). In this context, a previous study reported that Cdk1 phosphorylates CAP-D3 at Thr1415 and that this phosphorylation promotes the further phosphorylation of the condensin II complex by Plk1 (Abe et al., 2011). Notably, nonphosphorylatable CAP-D3 at Thr1415 impairs condensin II activity but not chromosomal recruitment durin g mitosis (Abe et al., 2011). In contrast, the chromosomal localization of condensin I was largely dependent on the phosphorylation of CAP-H at Ser70 by Aurora B (Tada et al., 2011). CAP-H2 and CAP-H belong to the "kleisin" protein superfamily, both of which conserve the structural similarities. These findings thus suggest the possibility that the chromosomal recruitment of condensins depends on the phosphorylations of kleisin family proteins. Importantly, there is no evidence that Aurora B has any role for the regulation of condensin II (Lipp et al., 2007). In this regard, we show for the first time that Mps1 kinase controls the chromosomal localization of condensin II.

Accumulating lines of evidence have revealed the molecular mechanisms by which Mps1 controls chromosome dynamics, including chromosome alignment and segregation (Liu and Winey, 2012). The current study uncovers a novel Mps1 function in the maintenance of the chromosome architecture, including condensation. Ser492 of CAP-H2 is phosphorylated by Mps1, and this phosphorylation is required for prophase chromosome condensation (Fig. 5 F). Defects in the chromosome structure cause chromosome segregation errors during anaphase and genome instability. In this regard, the processes that regulate mitotic chromosome condensation are also crucial for genome stability. Taken together, we conclude that Mps1 functions in not only the regulation of chromosome dynamics but also chromosome structures through the process of mitosis to maintain genome stability.

Materials and methods

Cell culture and cell synchronization

HeLa cells and 293 cells were cultured in DMEM containing 10% heat-inactivated FBS, penicillin, and streptomycin. Cells were maintained at 37°C in 5% CO_2. To synchronize at mitosis, cells were treated with 30 ng/ml nocodazole (Sigma-Aldrich). In some experiments, cells were treated with 200 ng/ml nocodazole and 10 µM MG132. Mitotic cells were collected in suspension by gently shaking cells off the culture dishes (mitotic shake-off method). To synchronize at the G1/S phase, HeLa cells were synchronized using a double thymidine block method. Cells were treated with 2 mM thymidine (Wako Pure Chemical Industries, Ltd.) for 14 h, washed twice with fresh medium, and released for 10 h. Thymidine was added again to a final concentration of 2 mM to synchronize cells at the G1/S phase.

Preparation of a phospho-specific antibody

To generate a phospho-specific antibody against Ser492-phosphorylated CAP-H2, phosphopeptides (QETEL(pS)QRIRD) were used to immunize rabbits (Operon). The anti-serum was affinity purified against the phosphorylated peptides.

Immunoblot and immunoprecipitation

Cells were harvested, washed in PBS, and resuspended in lysis buffer (50 mM Tris-HCl, pH 7.6, 150 mM NaCl, 1 mM PMSF, 1 mM DTT, 10 µg/ml aprotinin, 1 µg/ml leupeptin, 1 µg/ml pepstatin A, and 1% NP-40) with phosphatase inhibitor (10 mM NaF and 1 mM Na_3VO_4). After centrifugation, the supernatants were isolated and used as cell lysates. To obtain whole-cell lysate, cells were suspended in SDS-lysis buffer (50 mM Tris-HCl, pH 7.6, 150 mM NaCl, 1 mM PMSF, 1 mM DTT, 10 µg/ml aprotinin, 1 µg/ml leupeptin, 1 µg/ml pepstatin A, 1% SDS, and 1% NP-40) and sonicated. Lysates were incubated with normal rabbit IgG (Santa Cruz Biotechnology, Inc.), rabbit anti-Mps1 (Santa Cruz Biotechnology, Inc.), or rabbit anti-SMC2 (Bethyl Laboratories, Inc.) for 1 h at 4°C. Then, the solutions were incubated with protein A–Sepharose CL-4B (GE Healthcare) for 2 h at 4°C. For the immunoprecipitation of GFP-tagged proteins, lysates were incubated with anti-GFP agarose (Medical & Biological Laboratories Co.). For the immunoprecipitation of Flag-tagged proteins, lysates were incubated with anti-Flag agarose (Sigma-Aldrich). The beads were washed three times in lysis buffer and resuspended in lysis buffer. Cell lysates and immunoprecipitated proteins were boiled for 5 min, separated by SDS-PAGE, and transferred onto nitrocellulose membranes. The membranes were blocked with Blocking One (Nacalai Tesque), washed three times in PBS with 0.05% Tween 20, incubated with rabbit anti-SMC2 (Bethyl Laboratories, Inc.), rabbit anti-Mps1 (Santa Cruz Biotechnology, Inc.), mouse anti–cyclin E (Santa Cruz Biotechnology, Inc.), mouse anti-tubulin (Sigma-Aldrich), rabbit anti-SMC4 (Bethyl Laboratories, Inc.), rabbit anti–CAP-H (Bethyl Laboratories, Inc.), rabbit anti–CAP-H2 (Bethyl Laboratories, Inc.), rabbit anti–CAP-G2 (Bethyl Laboratories, Inc.), rabbit anti–CAP-D3 (Bethyl

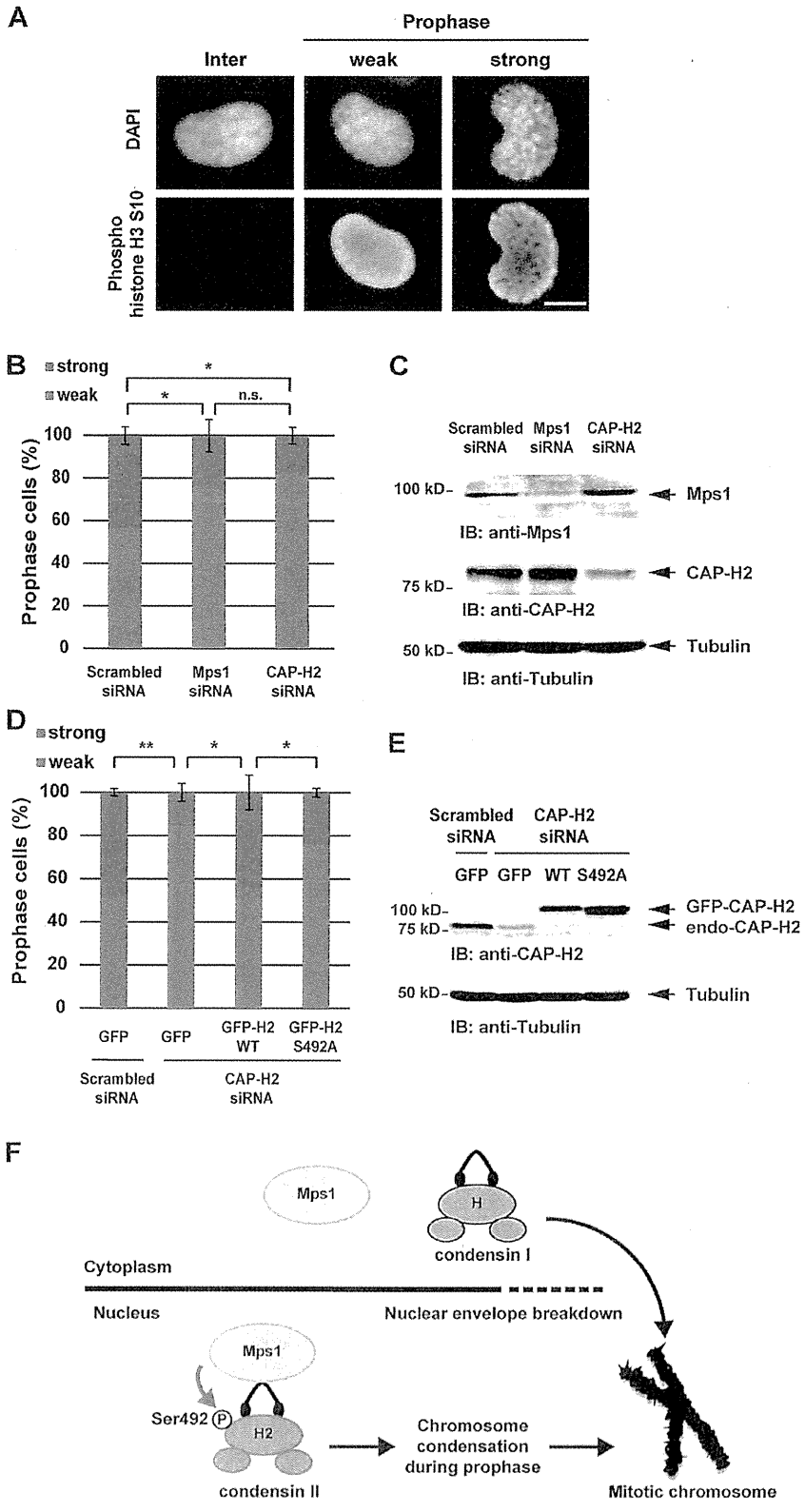

Figure 5. **Mps1 regulates chromosome condensation during prophase.** (A) Fixed HeLa cells were stained with anti–phospho-histone H3 Ser10. DNA was stained by DAPI. Degrees of prophase condensation were defined in the two categories and the representative cells are shown. Bar, 10 μm. (B) HeLa cells were transfected with the indicated siRNAs and fixed. The percentage of each category, as defined in A, was calculated. Data represent the mean ± SD from three independent experiments (*, $P < 0.05$; n.s., not significant). (C) The efficiency of protein depletion by siRNAs in B was analyzed by immunoblotting. (D) GFP, GFP-CAP-H2-WT, or GFP-CAP-H2-S492A cell lines were transfected with scrambled siRNA or CAP-H2 siRNA and fixed. The percentage of each category, as defined in A, was calculated. Data represent the mean ± SD from three independent experiments (*, $P < 0.05$; **, $P < 0.01$). (E) The efficiency of protein depletion by siRNA in D was analyzed by immunoblotting. (F) A model of condensin II regulation by Mps1. Mps1 interacts with condensin II in the nucleus during the cell cycle. In the early phase of mitosis, Mps1 phosphorylates CAP-H2 at Ser492 and recruits condensin II on chromatin to induce mitotic chromosome condensation.

Laboratories, Inc.), rabbit anti–phospho-histone H3 Ser10 (EMD Millipore), mouse anti-GFP (Nacalai Tesque), rabbit anti-Flag (Cell Signaling Technology), rabbit anti–lamin B1 (Santa Cruz Biotechnology, Inc.), mouse anti-ORC2 (Medical & Biological Laboratories Co.), or rabbit anti–phospho-CAP-H2-Ser492. Membranes were then washed three times in PBS with 0.05% Tween 20, incubated with peroxidase-conjugated anti–rabbit IgG (Santa Cruz Biotechnology, Inc.) or peroxidase-conjugated anti–mouse IgG (Santa Cruz Biotechnology, Inc.), and washed three times in PBS with 0.05% Tween 20. Immune complexes were visualized by using a Western Lightning Plus-ECL substrate (PerkinElmer).

Silver staining and mass spectrometric analysis

Silver staining was performed using Silver Stain Plus (Bio-Rad Laboratories). The gels were analyzed for mass spectrometry, which was performed by the Cellular and Proteome Research Laboratory, Medical Research Institute, Tokyo Medical and Dental University (Tokyo, Japan). To identify phosphorylation sites on CAP-H2, a 2DICAL shotgun proteomics analysis was performed as described previously (Matsubara et al., 2009; Ono et al., 2009, 2012; Miyamoto et al., 2012). In brief, 2DICAL analyzed the data of mass-to-charge ratio (m/z), peak intensity, retention time (RT), and each sample generated by liquid chromatography and mass spectrometry as the elemental data; it deployed various two-dimensional images with different combinations of axes using these four elements. From the m/z-RT image, peaks derived from the same peptide in the direction of acquiring time were integrated. By adding algorisms to ensure reproducibility of m/z and RT, the same peak was compared precisely across different samples, and a statistical comparison of identical peaks in different samples led to the discovery of specific differentially expressed peptide peaks.

Subcellular fractionations

For nuclear and cytoplasmic fractionations, cells were harvested, washed in PBS, and resuspended in A buffer (10 mM Hepes, pH 7.6, 15 mM KCl, 2 mM $MgCl_2$, 0.1 mM EDTA, 1 mM DTT, 0.5 mM PMSF, and 10 µg/ml leupeptin). After centrifugation, the cell pellets were resuspended in B buffer (10 mM Hepes, pH 7.6, 15 mM KCl, 2 mM $MgCl_2$, 0.1 mM EDTA, 0.2% NP-40, 1 mM DTT, 0.5 mM PMSF, and 10 µg/ml leupeptin). After centrifugation, the supernatants were isolated and used as cytoplasmic lysates. The cell pellets were resuspended in S buffer (0.25 M sucrose, 10 mM Hepes, pH 7.6, 15 mM KCl, 2 mM $MgCl_2$, 0.1 mM EDTA, 1 mM DTT, 0.5 mM PMSF, and 10 µg/ml leupeptin). After centrifugation, the cell pellets were resuspended in D buffer (50 mM Hepes, 400 mM KCl, 0.1 mM EDTA, 10% glycerol, 1 mM DTT, 0.5 mM PMSF, and 10 µg/ml leupeptin). After centrifugation, the supernatants were isolated and used as nuclear lysates.

Chromosomal fractionation was performed as described previously (Méndez and Stillman, 2000). In brief, cells were harvested, washed in PBS, and resuspended in chromatin-A buffer (10 mM Hepes, 10 mM KCl, 1.5 mM $MgCl_2$, 0.34 M sucrose, 10% glycerol, 0.1% Triton X-100, 1 mM DTT, 0.5 mM PMSF, and 10 µg/ml leupeptin). The supernatants were isolated and used as S2 (soluble cytoplasmic fraction). The pellets were then washed in chromatin-A buffer and incubated in the absence or presence of micrococcal nucleases (New England Biolabs, Inc.) at 37°C for 2 min. After centrifugation, the pellets were resuspended in chromatin-B buffer (3 mM EDTA, 0.2 mM EGTA, 1 mM DTT, 0.5 mM PMSF, and 10 µg/ml leupeptin) and incubated on ice for 30 min. The supernatants were isolated and used as S3 (soluble nuclear fraction). The pellets were washed in chromatin-B buffer, added with Laemmli buffer, sonicated, boiled for 5 min, and centrifuged. The supernatants were isolated and used as P3 (chromosome fraction). P3 was used as the chromatin fraction, and the mixture of S2 and S3 was used as the soluble fraction.

In vitro kinase assay

Recombinant GST-CAP-H2 (Abnova) was incubated in kinase buffer (20 mM Hepes, 10 mM $MgCl_2$, 0.1 mM Na_3VO_4, and 2 mM DTT) with GST-Mps1 (Invitrogen) and ATP for 15 min. The reaction products were boiled for 5 min and subjected to immunoblot analysis.

siRNA transfections

The transfection of siRNA was performed using Lipofectamine RNAiMAX (Invitrogen) according to the manufacturer's instructions. The sequences of siRNAs were as follows: Mps1 siRNA, 5′-ugaacaaagugagagacauTT-3′ and 5′-augucucucacuuuguucaTT-3′; CAP-H2 siRNA1, 5′-gcugcaggacuucaccagTT-3′ and 5′-cugguggaaguccugcagcTT-3′; and CAP-H2 siRNA2, 5′-ggauuucaggaugaacacgTT-3′ and 5′-cguguucauccugaaauccTT-3′. Of note, the lowercase letters represent complementary RNA sequences for the target regions.

Plasmid construction and stable cell lines

GFP-Mps1 was constructed as described previously (Nihira et al., 2008). Mps1 cDNA was cloned into pEGFPC1 vector. Kinase-dead mutant of Mps1 (D664A) was generated by site-directed mutagenesis. CAP-H2 cDNA was cloned into the pEGFPC1 vector or the pcDNA3-Flag vector. Various mutations were introduced by site-directed mutagenesis. siRNA-resistant forms of CAP-H2 were generated by introducing silent mutations in the targeting regions for CAP-H2 siRNA1. To generate stable cell lines that express GFP-CAP-H2, HeLa cells were transfected with a plasmid encoding GFP-CAP-H2 using the X-tremeGENE 9 DNA transfection reagent (Roche). Stably expressing cell clones were selected by culture with medium containing G418.

Chromosome spreading

Cells were harvested, washed in PBS, resuspended in 75 mM KCl, and incubated for 15 min. Carnoy's fixative (methanol/acetic acid = 3:1) was added to the suspension. After washing twice with Carnoy's fixative, the cell pellets were resuspended in Carnoy's fixative. Fixed cells were dropped onto glass slides. An immunofluorescence analysis of spreading chromosomes was performed using rabbit anti–CAP-H2 (Bethyl Laboratories, Inc.).

Fluorescence microscopy

Cells cultured in chamber slides were fixed with 3% paraformaldehyde. Fixed cells were permeabilized with 1% Triton X-100 in PBS and incubated with 10% goat serum in PBS for 1 h. Cells were incubated with rabbit anti–phospho-histone H3 Ser10 (EMD Millipore) followed by a reaction with fluorescein isothiocyanate– or tetramethyl rhodamine isothiocyanate–conjugated secondary antibodies. DNA was stained with DAPI. Fixed cells were imaged at room temperature using an all-in-one type fluorescence microscope (Bio-Zero BZ-8000; Keyence) equipped with a Plan Apochromat 20×/0.75 NA objective lens (Nikon). Images were acquired with BZ Analyzer software (Keyence). Live cells were cultured in DMEM containing 10% FBS at 37°C in 5% CO_2 and were imaged using a DeltaVision Core system equipped with a microscope (IX71; Olympus), UPlan SApo 20×/0.75 NA objective lens (Olympus), and CoolSNAP HQ^2 camera (Photometrics). DNA was stained with 0.2 µg/ml Hoechst 33342. The living cell images were acquired with SoftWoRx software (Applied Precision). Imaging data were processed using Photoshop (Adobe).

Online supplemental material

Fig. S1 shows the purity of subcellular fractionations. Fig. S2 shows that Mps1 phosphorylates Ser492 of CAP-H2. Fig. S3 shows Ser492 phosphorylation during mitosis. Online supplemental material is available at http://www.jcb.org/cgi/content/full/jcb.201308172/DC1.

This work was supported by grants from the Ministry of Education, Science and Culture of Japan; the Jikei University Graduate Research Fund; the NOVARTIS Foundation for the Promotion of Science; Suzuken Memorial Foundation; Uehara Memorial Foundation; the Astellas Foundation for Research on Medical Resources; Takeda Science Foundation; the Mochida Memorial Foundation for Medical and Pharmaceutical Research; the Sumitomo Foundation; Japan Foundation for Applied Enzymology; Project Mirai Cancer Research grants; and the Naito Foundation.

The authors declare no competing financial interests.

Submitted: 30 August 2013
Accepted: 19 May 2014

References

Abe, S., K. Nagasaka, Y. Hirayama, H. Kozuka-Hata, M. Oyama, Y. Aoyagi, C. Obuse, and T. Hirota. 2011. The initial phase of chromosome condensation requires Cdk1-mediated phosphorylation of the CAP-D3 subunit of condensin II. *Genes Dev.* 25:863–874. http://dx.doi.org/10.1101/gad.2016411

Giet, R., and D.M. Glover. 2001. Drosophila aurora B kinase is required for histone H3 phosphorylation and condensin recruitment during chromosome condensation and to organize the central spindle during cytokinesis. *J. Cell Biol.* 152:669–682. http://dx.doi.org/10.1083/jcb.152.4.669

Hirano, T. 2012. Condensins: universal organizers of chromosomes with diverse functions. *Genes Dev.* 26:1659–1678. http://dx.doi.org/10.1101/gad.194746.112

Hirota, T., D. Gerlich, B. Koch, J. Ellenberg, and J.M. Peters. 2004. Distinct functions of condensin I and II in mitotic chromosome assembly. *J. Cell Sci.* 117:6435–6445. http://dx.doi.org/10.1242/jcs.01604

Jelluma, N., A.B. Brenkman, N.J. van den Broek, C.W. Cruijsen, M.H. van Osch, S.M. Lens, R.H. Medema, and G.J. Kops. 2008. Mps1 phosphorylates

Borealin to control Aurora B activity and chromosome alignment. *Cell.* 132:233–246. http://dx.doi.org/10.1016/j.cell.2007.11.046

Kemmler, S., M. Stach, M. Knapp, J. Ortiz, J. Pfannstiel, T. Ruppert, and J. Lechner. 2009. Mimicking Ndc80 phosphorylation triggers spindle assembly checkpoint signalling. *EMBO J.* 28:1099–1110. http://dx.doi.org/10.1038/emboj.2009.62

Kimura, K., M. Hirano, R. Kobayashi, and T. Hirano. 1998. Phosphorylation and activation of 13S condensin by Cdc2 in vitro. *Science.* 282:487–490. http://dx.doi.org/10.1126/science.282.5388.487

Leng, M., D.W. Chan, H. Luo, C. Zhu, J. Qin, and Y. Wang. 2006. MPS1-dependent mitotic BLM phosphorylation is important for chromosome stability. *Proc. Natl. Acad. Sci. USA.* 103:11485–11490. http://dx.doi.org/10.1073/pnas.0601828103

Lipp, J.J., T. Hirota, I. Poser, and J.M. Peters. 2007. Aurora B controls the association of condensin I but not condensin II with mitotic chromosomes. *J. Cell Sci.* 120:1245–1255. http://dx.doi.org/10.1242/jcs.03425

Liu, X., and M. Winey. 2012. The MPS1 family of protein kinases. *Annu. Rev. Biochem.* 81:561–585. http://dx.doi.org/10.1146/annurev-biochem-061611-090435

London, N., S. Ceto, J.A. Ranish, and S. Biggins. 2012. Phosphoregulation of Spc105 by Mps1 and PP1 regulates Bub1 localization to kinetochores. *Curr. Biol.*22:900–906. http://dx.doi.org/10.1016/j.cub.2012.03.052

Matsubara, J., M. Ono, A. Negishi, H. Ueno, T. Okusaka, J. Furuse, K. Furuta, E. Sugiyama, Y. Saito, N. Kaniwa, et al. 2009. Identification of a predictive biomarker for hematologic toxicities of gemcitabine. *J. Clin. Oncol.* 27: 2261–2268. http://dx.doi.org/10.1200/JCO.2008.19.9745

Méndez, J., and B. Stillman. 2000. Chromatin association of human origin recognition complex, cdc6, and minichromosome maintenance proteins during the cell cycle: assembly of prereplication complexes in late mitosis. *Mol. Cell. Biol.* 20:8602–8612. http://dx.doi.org/10.1128/MCB.20.22.8602-8612.2000

Miyamoto, T., N. Kitamura, M. Ono, Y. Nakamura, M. Yoshida, H. Kamino, R. Murai, T. Yamada, and H. Arakawa. 2012. Identification of 14-3-3γ as a Mieap-interacting protein and its role in mitochondrial quality control. *Sci Rep.* 2:379. http://dx.doi.org/10.1038/srep00379

Nihira, K., N. Taira, Y. Miki, and K. Yoshida. 2008. TTK/Mps1 controls nuclear targeting of c-Abl by 14-3-3-coupled phosphorylation in response to oxidative stress. *Oncogene.* 27:7285–7295. http://dx.doi.org/10.1038/onc.2008.334

Ono, M., J. Matsubara, K. Honda, T. Sakuma, T. Hashiguchi, H. Nose, S. Nakamori, T. Okusaka, T. Kosuge, N. Sata, et al. 2009. Prolyl 4-hydroxylation of alpha-fibrinogen: a novel protein modification revealed by plasma proteomics. *J. Biol. Chem.*284:29041–29049. http://dx.doi.org/10.1074/jbc.M109.041749

Ono, M., M. Kamita, Y. Murakoshi, J. Matsubara, K. Honda, B. Miho, T. Sakuma, and T. Yamada. 2012. Biomarker discovery of pancreatic and gastrointestinal cancer by 2DICAL: 2-dimensional image-converted analysis of liquid chromatography and mass spectrometry. *Int. J. Proteomics.* 2012: 897412. http://dx.doi.org/10.1155/2012/897412

Ono, T., Y. Fang, D.L. Spector, and T. Hirano. 2004. Spatial and temporal regulation of Condensins I and II in mitotic chromosome assembly in human cells. *Mol. Biol. Cell.* 15:3296–3308. http://dx.doi.org/10.1091/mbc.E04-03-0242

Shepperd, L.A., J.C. Meadows, A.M. Sochaj, T.C. Lancaster, J. Zou, G.J. Buttrick, J. Rappsilber, K.G. Hardwick, and J.B. Millar. 2012. Phospho-dependent recruitment of Bub1 and Bub3 to Spc7/KNL1 by Mph1 kinase maintains the spindle checkpoint. *Curr. Biol.* 22:891–899. http://dx.doi.org/10.1016/j.cub.2012.03.051

Shimogawa, M.M., B. Graczyk, M.K. Gardner, S.E. Francis, E.A. White, M. Ess, J.N. Molk, C. Ruse, S. Niessen, J.R. Yates III, et al. 2006. Mps1 phosphorylation of Dam1 couples kinetochores to microtubule plus ends at metaphase. *Curr. Biol.* 16:1489–1501. http://dx.doi.org/10.1016/j.cub.2006.06.063

St-Pierre, J., M. Douziech, F. Bazile, M. Pascariu, E. Bonneil, V. Sauvé, H. Ratsima, and D. D'Amours. 2009. Polo kinase regulates mitotic chromosome condensation by hyperactivation of condensin DNA supercoiling activity. *Mol. Cell.* 34:416–426. http://dx.doi.org/10.1016/j.molcel.2009.04.013

Stucke, V.M., H.H. Silljé, L. Arnaud, and E.A. Nigg. 2002. Human Mps1 kinase is required for the spindle assembly checkpoint but not for centrosome duplication. *EMBO J.*21:1723–1732. http://dx.doi.org/10.1093/emboj/21.7.1723

Tada, K., H. Susumu, T. Sakuno, and Y. Watanabe. 2011. Condensin association with histone H2A shapes mitotic chromosomes. *Nature.* 474:477–483. http://dx.doi.org/10.1038/nature10179

Takemoto, A., A. Murayama, M. Katano, T. Urano, K. Furukawa, S. Yokoyama, J. Yanagisawa, F. Hanaoka, and K. Kimura. 2007. Analysis of the role of Aurora B on the chromosomal targeting of condensin I. *Nucleic Acids Res.* 35:2403–2412. http://dx.doi.org/10.1093/nar/gkm157

Yamagishi, Y., C.H. Yang, Y. Tanno, and Y. Watanabe. 2012. MPS1/Mph1 phosphorylates the kinetochore protein KNL1/Spc7 to recruit SAC components. *Nat. Cell Biol.*14:746–752. http://dx.doi.org/10.1038/ncb2515

Proteomic analysis of ligamentum flavum from patients with lumbar spinal stenosis

Masahiro Kamita[1], Taiki Mori[2], Yoshihito Sakai[3], Sadayuki Ito[3], Masahiro Gomi[4], Yuko Miyamoto[1], Atsushi Harada[3], Shumpei Niida[2], Tesshi Yamada[1], Ken Watanabe[5], Masaya Ono[1]*

[1]Division of Chemotherapy and Clinical Research, National Cancer Center Research Institute, 5-1-1 Tsukiji, Chuo-ku, Tokyo, 104-0045, Japan.

[2]BioBank Omics Unit, National Center for Geriatrics and Gerontology (NCGG), 35 Gengo, Morioka, Obu, Aichi 474-8511, Japan.

[3]Department of Orthopedic Surgery, NCGG, 35 Gengo, Morioka, Obu, Aichi 474-8511, Japan.

[4]BioBusiness Group, Mitsui Knowledge Industry, Tokyo, 164-8555 Japan.

[5]Department of Bone and Joint Disease, NCGG, 35 Gengo, Morioka, Obu, Aichi 474-8511, Japan.

*To whom correspondence should be addressed: Dr. Masaya Ono, 5-1-1 Tsukiji, Chuo-ku, Tokyo, 104-0045, Japan. Phone: +81-3-3542-2511; Fax: +81-3-3542-2511; E-mail: masono@ncc.go.jp

Abbreviations: LSS, Lumbar spinal stenosis; LF, Ligamentum flavum; 2DICAL, 2-dimensional image converted analysis of LC/MS

Key words: 2-dimensional image converted analysis of LC/MS, Ligamentum flavum, Lumbar spinal stenosis

Total number of words: 4948 words

Received: 16-Sep-2014; Revised: 16-Nov-2014; Accepted: 08-Jan-2015

This article has been accepted for publication and undergone full peer review but has not been through the copyediting, typesetting, pagination and proofreading process, which may lead to differences between this version and the Version of Record. Please cite this article as doi: 10.1002/pmic.201400442.

Abstract

Lumbar spinal stenosis (LSS) is a syndromic degenerative spinal disease and is characterized by spinal canal narrowing with subsequent neural compression causing gait disturbances. Although LSS is a major age-related musculoskeletal disease that causes large decreases in the daily living activities of the elderly, its molecular pathology has not been investigated using proteomics. Thus, we used several proteomic technologies to analyze the ligamentum flavum (LF) of individuals with LSS. Using comprehensive proteomics with SCX fractionation, we detected 1,288 proteins in these LF samples. A GO analysis of the comprehensive proteome revealed that more than 30% of the identified proteins were extracellular. Next we used 2-dimensional image converted analysis of LC/MS (2DICAL) to compare LF obtained from individuals with LSS to that obtained from individuals with disc herniation (non-degenerative control). We detected 64,781 MS peaks and identified 1675 differentially expressed peptides derived from 286 proteins. We verified four differentially expressed proteins (fibronectin, serine protease HTRA1, tenascin, and asporin) by quantitative proteomics using SRM/MRM. The present proteomic study is the first to identify proteins from degenerated and hypertrophied LF in LSS, which will help in studying LSS.

1. Introduction

Lumbar spinal stenosis (LSS) is a syndromic degenerative spinal disease and is characterized by spinal canal narrowing with possible subsequent neural compression causing gait disturbances such as intermittent claudication [1-3]. LSS is a major age-related musculoskeletal disease that causes large decreases in the activities of daily living of the elderly, and it is the most frequent indication for spinal surgery in elderly patients [1, 2, 4]. In Japan, the prevalence of symptomatic LSS in the elderly has been estimated at 3.65–5.7 million people among the whole population [5, 6]. Despite the importance of this disease, its etiology and molecular pathology have not been well described. Consequently, other than spine surgery, the therapeutic options for LSS are limited.

Multiple factors might contribute to narrowing of the spinal canal spaces [1-3]. For example, a thickened ligamentum flavum (LF), facet deformation, or intervertebral disk protrusion can all lead to stenosis of the spinal canal in LSS. LF is a ligament that lines the dorsal side of the spinal canal and connects the upper and lower vertebra and, unlike the collagen fibers of other tendons and ligaments, it mainly comprises elastic fibers [7, 8]. There have been several attempts to describe the molecular pathology of hypertrophied LF using the same approaches used to investigate the phenomena observed in aging and degeneration of elastic tissues such as blood vessels and skin [9-12]; however, a non-biased approach has not yet been described.

Non-biased approaches such as genomics, transcriptomics, metabolomics, and proteomics have recently been used to determine the etiologies of several human diseases. In the discovery of biomarkers and development of drugs, the key technology is proteomics using gel-based, antibody-based, and MS-based analyses [13]. In particular, shotgun proteomics, which uses nanoflow liquid chromatography coupled with high-resolution MS (LC/MS), is a powerful tool for detecting the protein components of a cell and have also been used to comprehensively identify

proteins associated with human diseases [14]. Shotgun proteomics can be used to typically detect several thousand proteins in multiple samples, but without labeling, and it cannot directly compare the amount of proteins between several samples.

In our laboratory, the mass spectrometric peak data, which are indicated by retention time, m/z, and sample intensity, are compared without an unconventional reagent using an in-house software, 2-dimensional image converted analysis of LC/MS (2DICAL). This software first detects the MS peaks that have a different intensity compared with a control and then identifies these peaks via a protein sequence database such as SwissProt. Therefore, 2DICAL allows selection of the differentially expressed peptides or proteins from the thousands detected using shotgun proteomics [15]

Here, we focused on the degeneration and hypertrophy of LF in LSS. Specifically, we used comprehensive proteomics with an SCX principle to analyze the molecular components of LF. Following comprehensive proteomics, we compared LF in individuals with LSS with that in individuals with disc herniation (non-degenerative control) using 2DICAL to identify differently expressed proteins and used quantitative proteomics with SRM/MRM to verify the identified proteins. To the best of our knowledge, this is the first report of proteomic identification of proteins from degenerated and hypertrophied LF in LSS.

2. Materials and methods

2.1 Patient groups and clinical samples

Seventy-three LF samples were obtained with written informed consent from patients with LSS (subjects) and with lumbar disc herniation [LDH; the non-degenerative control (controls)] during their surgical procedures at National Center for Geriatrics and Gerontology (NCGG) between 2010 and 2011. The LF samples were provided by Biobank, NCGG. The LSS group included 54 patients with LSS, with 34 (17 males and 17 females; mean age = 72.9 years) and 20 (11 males and 9 females; mean age = 70.7 years) patients recruited in 2010 and 2011, respectively. The control group included 19 participants, with 7 (4 males, 3 females; mean age = 42.4 years) and 12 (7 males, 5 females; mean age = 45.5 years) patients recruited in 2010 and 2011, respectively. The LF samples are listed in detail in Supplementary Table 1. The study was reviewed and approved by the institute's Ethics Committee.

2.2 Sample preparation for comparative proteomics and targeted proteomics

The LF samples (approximately 5 mg) were disrupted using a Shake Master auto machine (BioMedical Science Inc., Tokyo, Japan) and soaked in 500 μL of methanol until trypsin digestion. The soaked samples were then dried and digested in a solution containing 2-M Urea, 50-mM NH_4HCO_3, 1% Sodium deoxycholate (SDC), and 2-μg trypsin at 37 °C for 14 h with gentle agitation. The digests were treated by the phase-transfer method for SDC removal [16]. The obtained peptides were resolved with 0.1% formic acid (FA) and then quantified using a Qubit® Protein Assay Kit (Life technologies, Carlsbad, CA). For the shotgun proteomics coupled with 2DICAL, 3 μg of peptide solution was desalted according to the protocol described in C18 StageTip [17], dried, and resolved in 20 μL of 0.1% FA. The obtained peptide solution (2 μL) was subjected to splitless nanoLC (Hitachi High-Technologies, Japan) coupled with TripleTOF®5600 (AB SCIEX, Framingham, MA). For the targeted proteomics by SRM/MRM, the same desalted peptide was dried and then resuspended in solution (20 μL of 0.1% FA containing 50 fmol/μL of an internal standard peptide). Finally, samples were subjected to nanoLC-Ultra 2D (AB SCIEX, Framingham, MA) or Nexera UHPLC/HPLC System (Shimazu, Kyoto, Japan) coupled with QTRAP®5500 (AB SCIEX, Framingham, MA).

2.3 Comprehensive proteomics using StageTip-based SCX fractionation

In total, 3 μg of tryptic digest was separated into five fractions by StageTip-based SCX fractionation. Briefly, the SCX-Tip was assembled by stacking each layer of a 3M Cation-exchange disk, followed by a 3M Empore C18 disk in a dispensable 200-μL micropipette tip. The fractionation procedure was performed according to Nature Protocol [18]. The loaded peptides were eluted with a solution comprising 20% ACN, 0.1% FA, and several concentrations of ammonium acetate (50, 100, 150, 250, and 500 mM) added in a stepwise manner. The stepwise eluted fractions were desalted using C18 StageTip. Each fraction containing peptides (300 ng) was subjected to nanoLC-Ultra 2D with TripleTOF5600. The fractionated peptides were directly injected into a C18 reverse-phase column (75 μm × 150 mm; ChromXP C18-CL 3 μm 120 Å; Ekisigent, Redwood City, CA) equipped in nanoLC-Ultra 2D and then separated by a binary gradient consisting of the mobile phase (A) 0.1% FA and 1% ACN and the mobile phase (B) 0.1% FA and 99 % ACN. The gradient condition was as follows: 2% of B initially was increased to 25% of B at 130 min, to 90% of B at 131 to 135 min, and to 2% of A at 135.1 min (total run time of 155 min). The masses of the eluted peptides were determined using TripleTOF5600. All MS/MS data were combined and searched using the Protein Pilot software (AB SCIEX, Redwood City, CA). The Protein Pilot search comprised the following parameters: (1) digestion, trypsin; ID focus, biological modifications; database, last SwissProt release; species filtering, Homo sapiens; search effort, through ID; and detection protein threshold unused ProtScore, >0.47 (60%). The identified proteins were classified by GO Slims, and their representative graphs were constructed using R version 2.12.0 (http://www.r-project.org/index.html).

2.4 2DICAL-based label-free comparative proteomics

The desalted peptide samples were analyzed in duplicate using a NanoFrontier nanoLC connected to a TripleTOF5600. MS peaks were detected and quantified using the in-house 2DICAL software, as described previously [15]. A peak identification number was assigned to each MS peak (1 to 64,781). To identify the proteins, the MS and MS/MS data were searched using the Mascot software (version 2.4.1; Matrix Science; London, UK) using the Uniprot/Swiss-Prot database against a human database (Homo sapiens, 471,472 sequences in Sprot_57.5 fasta file). A heat map of differentially detected peptides was constructed using R 2.12.0.

2.5 Quantitation of differentially expressed peptides by SRM/MRM

The desalted peptides were separated using the NanoLC Ultra 2D system equipped with a trap column (200 μm × 0.5 mm, chromXP C18-CL 3 μm 120 Å; Ekisigent) and a C18 reverse-phase column for quantitation of fibronectin, serine protease HTRA1, and tenascin. A binary gradient comprising mobile phases A and B was used to separate the peptides. The gradient condition was as follows: 2% of B initially was increased to 50% of B at 20 min, to 80% of B at 21 to 25 min, and to 2% of B at 25.1 min (total run time of 40 min). For asporin quantitation, separation was performed using the Nexera UHPLC/HPLC System equipped with an XBridge BEH C18 column (2.1 × 100 mm; BEH C18 2.5 μm; Waters, Milford, MA) to use TurboV sourceTM. The separated and eluted peptides were detected using QTRAP5500 with multiplexed SRM/MRM transitions and MS conditions (Supplementary Table 2). A standard curve was generated using a solution equally mixed with the serial dilutions of a light peptide (0, 25, 50, 100, and 200 fmol/μL) and an internal standard heavy peptide (50 fmol/μL). The quantitation value was calculated for each transition from the ratio of the peak areas of the light and heavy peptides.

2.6 Immunohistochemical analyses

Immunohistochemical staining was performed of 6-μm paraffin-embedded LF sections fixed in 3% paraformaldehyde. The sections were deparaffinized and washed in PBS. Tissue sections were quenched in 3% hydrogen peroxide and methanol and then blocked with PBS/5% goat serum. Slides of each tissue section were incubated overnight at 4 °C with rabbit polyclonal anti-fibronectin antibodies (1:200 dilution; Bioworld Technology, Inc., MN, U.S.A.), rabbit polyclonal anti-HTRA1 antibody (1:50 dilution; Abcam, Cambridge, U.K.), mouse monoclonal anti-tenascin antibody (1:100 dilution; Novus biological, CO, U.S.A.), or rabbit polyclonal anti-asporin antibody (1:50 dilution; Sigma-Aldrich, MO, U.S.A.). After washing, immunoreactivity was detected with a secondary antibody using Simple Stain MAX-PO (MULTI) reagent and DAB solution (NICHIREI Biosciences, Tokyo, Japan). Hematoxylin and eosin staining was used for counter staining, and Elastica van Gieson (EVG) staining was used to evaluate the elastic fibers.

3 Results

3.1 Characterization and identification of proteins in the LF of LSS samples using comprehensive proteomics

To investigate the molecular pathology of LF in LSS, we used comprehensive proteomics to examine LSS samples and two age-, sex-, and digested peptide concentration-matched control samples collected in 2010 and 2011. Overall, 1,288 proteins were identified with comprehensive proteomics using StageTip-based SCX fractionation. In total, 1,132 proteins were detected in the control samples and 894 were identified in LSS samples. As for unique proteins, 394 were detected in the control samples, 156 in LSS samples, and 738 in both control and LSS samples (Figure 1A). The identified proteins were categorized according to their cellular components in GO terms and then classified into 24 cellular components (Figure 1B). Figure 1C illustrates the cellular component categories for the unique proteins detected only in LSS samples. The unique proteins in LSS samples were especially related to extracellular regions (extracellular region, 21.1%; extracellular space, 8.1%, and proteinaceous extracellular matrix, 3.7%). All data for the identified proteins are presented in Supplementary Data 1 and 2.

3.2 Comparative proteomic analysis of LF samples obtained from controls and patients with LSS using 2DICAL

To identify the protein responsible for LF hypertrophy, a comparative proteomic analysis was conducted with 2DICAL using seven control samples and 34 LSS samples collected in 2010. According to the 2DICAL analysis, we detected 64,781 MS peaks with LC/MS and identified 1,675 differentially expressed peptides derived from 286 proteins using LC/MS/MS (Figure 2A and Supplementary Data 3).

Figure 2B and C shows box plots and intensity maps of each MS peak. This figure also illustrates an example of a differentially expressed peptide, Peak ID 96, that had a 440.848 m/z and 48.368 retention time and compared with the control samples, its levels were clearly increased in LSS samples. This peak was identified as serine protease HTRA1. Similarly, differentially expressed peptides identified in LSS samples at levels either two-fold higher or lower than those in control samples were searched with 2DICAL and included in the heat map (Figure 3). LSS samples contained 281 peptides derived from 67 proteins, expressed at levels that were at least two-fold higher than those in control samples; the control samples contained 35 peptides derived from 10 proteins, expressed at levels higher than those in LSS samples (indicated in the figure by an asterisk).

3.3 Verification of differentially expressed peptides using SRM/MRM with LC/MS/MS

To verify the results of the 2DICAL analysis, the amount of selected peptides expressed in 20 LSS and 12 control samples collected in 2011 was quantified with quantitative MS of SRM/MRM. For the SRM/MRM analysis, we selected four peptides that were derived from fibronetin, HTRA1, tenascin, and asporin, because they contained many peptide fragments in which the upward or downward trend in the level of peptides were the same between the control and LSS samples; in addition, ionization of the selected peptides was predicted to be high by ESPPredictor [19]. The expression levels of fibronectin (24.775 ± 31.241 vs. 6.251 ± 3.121, $p = 0.019$), HTRA1 (46.515 ± 47.270 vs. 6.333 ± 5.152, $p = 0.002$), and tenascin (10.192 ± 14.844 vs. 1.654 ± 1.158, $p = 0.022$) were significantly higher in LSS samples than in control samples (Figure 4A–C). In contrast, asporin was expressed at higher levels in controls than in LSS samples (47.129 ± 25.694 vs. 23.602 ± 25.558, $p = 0.029$; Figure 4D). These results confirmed that 2DICAL correctly identified the differentially expressed peptides. The expression levels of fibronectin, HTRA1, and tenascin correlated positively and that of asporin correlated negatively with the thickness of LF (Supplementary Tables 3 and 4).

3.4 Immunohistochemistry of differentially expressed proteins

We performed an immunohistological assessment of the differentially expressed proteins to confirm the results of the SRM/MRM analysis. Typically, LF is an elastic tissue containing elastic fibers aligned with the fiber orientation (Figure 5A). In LSS, the elastic fibers decreased in number and became disorganized (Figure 5B). LF obtained from patients with LSS also showed increased staining for fibronectin and HTRA1 and included regions of the junctional areas between fibrocartilage and core ligaments (Figure 5C–F). Tenascin was immunolocalized in regions where the elastic fibers were lost, but it was not present in the ligaments of controls, which contained densely aligned elastic fibers (Figure 5G and H). Asporin was detected in the ligaments of controls, but the signal was decreased and diffused in the ligaments of LSS samples (Figure 5I–J). The results of the proteomic analysis were consistent with the in vivo finding

4. Discussion

Ligaments and tendons are primarily composed of collagen bundles and have fewer cellular contents than other tissues [20]. LF is known as the tissue predominantly containing enriched elastic fiber composed of elastin [12]. Hence, general one-shot proteomics could not identify a variety of proteins in LF. Identifying a large number of proteins in LF required a procedure that both completely solubilizes the tissue and avoids being influenced by predominantly expressed proteins. By optimizing the procedure and fractionating digested peptides, as mentioned in Materials and Methods, 1288 proteins in LF were detected, although the number of identified proteins is still lower than the number detected in other tissues in modern proteomics. To obtain a more comprehensive proteome in LF, a new technology, such as that based on removing elastin and collagen or concentrating the specific cells related to LF, may be required.

In this study, the GO analysis on the comprehensive proteome of human LF consistently revealed that approximately 30% of the identified proteins were extracellular proteins. Collagen types I, III, and V, which are expressed in ligaments and tendons, and cartilaginous collagen types II, X, and XI were detected in both control and LSS samples. In addition to the typical collagens, uncommon collagens such as types VI, VIII, XV, XVI, and XVIII, as well as fibril-associated collagens with interrupted triple helices (types XII, XIV, and XXI), were identified in LF. Moreover, small leucine-rich proteoglycans expressed in ligaments and tendons, such as asporin, decorin, biglycan, lumican, podocan, and fibromodulin [21], as well as the large proteoglycans versican and aggrecan, were identified in LF. Such a composition suggests that LF shares features with other ligaments and tendons. LF is one of the most elastic ligaments among the ligaments and tendons in the human body [22, 23]. This feature is reflected by the many elastic fibers identified in the proteomic analysis, such as elastin, fibulins (FBLN1, FBLN2, FBLN3, and FBLN5), and MFAP4. SOD3 and LOXL1, redox

proteins that participate in elastic fiber formation and regulation [24, 25], are also present in LF. Information regarding the proteins expressed in LF is limited; therefore, most proteins identified in this study were not previously identified in LF. Thus, our study provides a useful and detailed list of proteins expressed in human LF, a tissue that is largely uncharacterized at the molecular level.

The 2DICAL-based differential proteomic approach revealed the profile of degenerative LF present in LSS. Blood plasma proteins such as apolipoproteins, fibrinogens, and transthyretin were significantly increased in the LF of LSS samples. This observation is consistent with the anatomical changes occurring in hypertrophied LF that also increase the vasculature in degenerative ligaments [26]. Proteins known as cartilage elements were also increased in LSS samples; chondroadherin, prolargin/PRELP, CILPs, and aggrecan were markedly upregulated in LSS samples. It is widely recognized that chondrometaplasia is often observed in degenerated LF [22]. Because the enthesis and hard tissue moieties (cartilages and bones) were mostly eliminated from the LF samples subjected to the proteomic analysis, the increase in cartilage proteins in LSS may reflect the development of chondrometaplasia. In addition, the elastic fiber components FBLN5 and MFAP4 decreased significantly as the elastic fiber organization in the LSS samples decreased. Furthermore, asporin plays a protective role against periodontal mineralization [27]. Degenerative LF is often mineralized, which implies that a decrease in asporin is associated with LF calcification. Taken together, the proteome findings accurately describe the pathological transitions that occur in the extracellular matrix of LF with identifying the proteins involved. At the same time, our study has not been able to directly demonstrate whether the identified proteins are biologically related to the pathogenesis of LSS. Although earlier studies have tried to characterize LF using primary cultured LF cells from patients with LSS [28, 29], these cultures were rich in various cell types, having the potential to lead to ambiguous results. Therefore, the biological relevance of proteins associated with LSS could not be determined using primary cultured LF cells. Matsumoto et al. recently constructed rare disease model cells using human induced pluripotent stem (iPS) cells derived from patients with fibrodysplasia ossificans progressive [30]. If an LF model cell characterizing the pathogenesis of LSS can be similarly constructed using the iPS technology, it may enable us to reveal the relationship of the identified proteins with LSS.

The MRM analysis confirmed that, among the differentially expressed proteins, expressions of fibronectin, HTRA1, and tenascin were increased, whereas that of asporin was decreased, in the LF

of LSS samples. The levels of peptides derived from fibronectin positively correlated with those derived from HTRA1 (correlation coefficient $r = 0.738$, $p < 0.0001$). The loss of function mutation in the HTRA1 gene leads to cerebral autosomal recessive arteriopathy with subcortical infarcts and leukoencephalopathy by dysregulating TGF-β signaling [31, 32]. Upregulation of HTRA1 was observed in age-related macular degeneration, osteoarthritis, and lumbar disc degeneration [33-36]. Grau et al. reported that HTRA1 processes fibronectin in arthritic joints [37]. Moreover, the fibronectin gene is a major target for TGF-β signaling. Tenascin is involved in wound healing as well as in lung and liver fibrosis, all of which are regulated by TGF-β signaling [38]. Similarly, a polymorphism of the asporin gene is associated with an increased incidence of osteoarthritis and causes a differential TGF-β response [39, 40]. The positive correlation between the levels of the proteins and the thickness of the ligaments suggested prolonged TGF-β signaling. It has been suggested that the expression of TGF-β is found in endothelial cells and is more pronounced in relatively early stages of degenerative hypertrophy of LF [10]. The study showed the expression of TGF-β1, a member of the TGF-β family, in the ligaments [10]. In the model of myocardial infarction, the expression of TGF-β1 and -β2 was observed in the early stages of fibrosis; expression of TGF-β3 was induced in and sustained during the later stages of hypertrophy [41]. Thus, there is a possibility that other members of the TGF-β family play a role in ligament hypertrophy. Further analysis is required to elucidate how TGF-β signaling is involved in hypertrophy of LF seen in LSS.

In the present study, several proteomic analyses revealed the molecular characteristics of LF and the differences between LF obtained from controls and patients with LSS. These findings will provide a useful and detailed list of proteins expressed in human LF.

Acknowledgement

This work was supported by the Program for Promotion of Fundamental Studies in Health Sciences conducted by the National Institute of Biomedical Innovation of Japan (10-44 and 10-45).

Conflict of interest

The authors have declared no conflict of interest.

5. Reference

[1] Katz, J.N., Harris, M.B., Clinical practice. Lumbar spinal stenosis. N. Engl. J. Med. 2008, 358, 818-825.

[2] Siebert, E., Pruss, H., Klingebiel, R., Failli, V. et al., Lumbar spinal stenosis: syndrome, diagnostics and treatment. Nat. Rev. Neurol. 2009, 5, 392-403.

[3] NASS evidence-based clinical guidelines committee: Diagnosis and treatment of degenerative lumbar spinal stenosis: evidence-based clinical guidelines for multidisciplinary spine care. North American Spine Society 2011.

[4] Lurie, J.D., Birkmeyer, N.J., Weinstein, J.N., Rates of advanced spinal imaging and spine surgery. Spine (Phila Pa 1976) 2003, 28, 616-620.

[5] Ishimoto, Y., Yoshimura, N., Muraki, S., Yamada, H. et al., Associations between radiographic lumbar spinal stenosis and clinical symptoms in the general population: the Wakayama Spine Study. Osteoarthritis Cartilage 2013, 21, 783-788.

[6] Yabuki, S., Fukumori, N., Takegami, M., Onishi, Y. et al., Prevalence of lumbar spinal stenosis, using the diagnostic support tool, and correlated factors in Japan: a population-based study. J. Orthop. Sci. 2013, 18, 893-900.

[7] Nachemson, A.L., Evans, J.H., Some mechanical properties of the third human lumbar interlaminar ligament (ligamentum flavum). J. Biomech. 1968, 1, 211-220.

[8] Brown, J.P., Lind, R.M., Burzesi, A.F., Kuo, C.K., Elastogenic protein expression of a highly elastic murine spinal ligament: the ligamentum flavum. PLoS One 2012, 7, 7.

[9] Kosaka, H., Sairyo, K., Biyani, A., Leaman, D. et al., Pathomechanism of loss of elasticity and hypertrophy of lumbar ligamentum flavum in elderly patients with lumbar spinal canal stenosis. Spine 1976, 32, 2805-2811.

[10] Sairyo, K., Biyani, A., Goel, V., Leaman, D. et al., Pathomechanism of ligamentum flavum hypertrophy: a multidisciplinary investigation based on clinical, biomechanical, histologic, and biologic assessments. Spine (Phila Pa 1976) 2005, 30, 2649-2656.

[11] Nakamura, T., Okada, T., Endo, M., Kadomatsu, T. et al., Angiopoietin-like protein 2 induced by mechanical stress accelerates degeneration and hypertrophy of the ligamentum flavum in lumbar spinal canal stenosis. PLoS One 2014, 9.

[12] Schrader, P.K., Grob, D., Rahn, B.A., Cordey, J. et al., Histology of the ligamentum flavum in patients with degenerative lumbar spinal stenosis. Eur. Spine. J. 1999, 8, 323-328.